Local structure in perovskite relaxor ferroelectrics by ^{207}Pb NMR

Donghua H. Zhou,[1] Gina L. Hoatson,[1,*] Robert L. Vold,[2] and Franck Fayon[3]

[1]*Department of Physics, College of William and Mary, P.O. Box 8795, Williamsburg, Virginia 23187-8795, USA*

[2]*Department of Applied Science, College of William and Mary, P.O. Box 8795, Williamsburg, Virginia 23187-8795, USA*

[3]*Centre de Recherche sur les Matériaux à Haute Température, CNRS,*
1D avenue de la Recherche Scientifique, 45071 Orléans Cedex 2, France

The ^{207}Pb static, magic-angle spinning (MAS), and two-dimensional phase-adjusted spinning sidebands (2D-PASS) NMR experiments have been performed on $(1-x)$PMN/xPSN [where PMN stands for Pb(Mg$_{1/3}$Nb$_{2/3}$)O$_3$ and PSN stands for Pb(Sc$_{1/2}$Nb$_{1/2}$)O$_3$] relaxor ferroelectrics. These materials have inherent chemical and positional disorder that results in very low-resolution static and MAS spectra. Only in 2D-PASS spectra can isotropic and anisotropic chemical shifts be separated. The isotropic chemical shift δ_{iso} ranges from -1800 to -900 ppm and the anisotropic chemical shift δ_{aniso} ranges from -700 to -230 ppm with asymmetry parameter η ranging from 0.5 to 1. Strong linear correlations between isotropic and anisotropic chemical shifts show that Pb-O bonds vary from more ionic to more covalent environments. The isotropic chemical shift measures the shortest Pb-O bond length and its distribution is quantitatively described. Such distribution is used to examine two competing models of Pb displacements; the direction of displacement is random in the spherical model but specific in the unique direction model. The spherical model is unable to yield the observed distribution of the shortest Pb-O bond length. The unique direction model may fit the observed distribution, but it is unable to discern the direction of the Pb displacement. This model fits experiments equally well with any given direction. However, the distribution parameters strongly depend on the direction; for PMN at 27 °C, $r_0(\sigma) = 0.455(0.039)$, 0.302(0.023), and 0.381(0.030) Å for [001], [011], and [111], respectively, where r_0 and σ are, respectively, the mean and standard deviation of the Gaussian distribution of the Pb displacement from the ideal position.

I. INTRODUCTION

Lead based perovskite relaxor ferroelectrics have very large dielectric, piezoelectric, and electromechanical responses and are important materials for capacitors, sensors, actuators, and transducers.[1–4] The microscopic origin of their macroscopic properties is still not well understood. The lead ion has large covalency and lone-pair electrons and should play an important role. For example in $A(B'_{1/3}B''_{2/3})$O$_3$ perovskites $(A=\mathrm{Ba}^{2+},\mathrm{Pb}^{2+}; \; B'=\mathrm{Mg}^{2+},\mathrm{Ca}^{2+},\mathrm{Zn}^{2+}; \; B''=\mathrm{Nb}^{5+},\mathrm{Ta}^{5+})$, 1:2 ordering of the two B cations is found along the [111] direction when the A ion is Ba^{2+}, while 1:1 ordering occurs when A is Pb^{2+}.[5] The Pb-based perovskites also have lower order-disorder transition temperatures than the Ba-based perovskites.[5] These phenomena have been attributed to the enhanced Pb-O hybridization between the Pb $6s$ and O $2p$ states of the underbonded oxygens in the B^{2+}-O-B^{2+} and B^{2+}-O-B^{5+} environments.[5,6] Similarly, the large covalency of Pb^{2+} compared to Ba^{2+} has been modeled by an environment-dependent effective A-site charge and it is able to explain the observed different ordering behaviors.[7]

It is clear from numerous experimental and theoretical investigations that there is an intimate connection in perovskite ceramics between A-site displacement and B-site disorder and distortion, with intriguing consequences for bulk piezoelectric and ferroelectric behavior.[8] Multinuclear NMR studies of one particular series of solid solutions can provide one piece of a complex puzzle. In order to accommodate

their lone-pair electrons, Pb^{2+} ions usually shift from high-symmetry positions. An x-ray-diffraction (XRD) study of Pb(Mg$_{1/3}$Nb$_{2/3}$)O$_3$ (PMN) shows that even at relatively high temperatures ($\sim$300 °C) lead ions are displaced from the perovskite cubic center.[9] The displacements may be random in both length and direction, but a spherical layer model (radius 0.285 and 0.259 Å for 20 and 300 °C, respectively) adequately describes the observed data.[9] However in Pb(Sc$_{1/2}$Ta$_{1/2}$)O$_3$ (PST), pair distribution function analysis (PDF) using neutron scattering and x-ray scattering shows that Pb^{2+} ions move (by 0.2 Å) in the [100] direction rather than the macroscopic polarization direction [111].[10] These results are very different and we hope this ^{207}Pb NMR study may shed some light on this issue.

We have studied local structures and quantitative B-site ordering of the solid solutions of PMN and Pb(Sc$_{1/2}$Nb$_{1/2}$)O$_3$ (PSN) using ^{93}Nb NMR.[11,12] In this work, the ^{207}Pb NMR of these solid solutions $(1-x)$PMN/xPSN is used to investigate the important role of Pb^{2+} ion. The chemical shielding tensor of ^{207}Pb measures the local magnetic fields created by molecular or crystal surroundings. In the principal-axis system (PAS), only the diagonal components δ_{11}, δ_{22}, and δ_{33} are nonzero. Conventionally, the chemical shielding tensor may be characterized by three parameters: the isotropic chemical shift δ_{iso}, the anisotropic shift δ_{aniso}, and the asymmetry parameter η. They are defined as

$$\delta_{\mathrm{iso}} = \tfrac{1}{3}(\delta_{11} + \delta_{22} + \delta_{33}),$$

$$\delta_{\text{aniso}} = \delta_{33} - \delta_{\text{iso}},$$

$$\eta = \frac{\delta_{22} - \delta_{11}}{\delta_{\text{aniso}}}, \tag{1}$$

where the principal components of the shielding tensor are arranged as $|\delta_{33} - \delta_{\text{iso}}| \geq |\delta_{11} - \delta_{\text{iso}}| \geq |\delta_{22} - \delta_{\text{iso}}|$.[13] This ordering places δ_{22} between δ_{11} and δ_{33}, and closer to δ_{11}. The parameter η ranges from 0 to 1 and measures the deviation from axial symmetry. The chemical shift anisotropy δ_{aniso} is a function of the relative orientation between the PAS and the laboratory frame. In powder samples, this orientation dependence produces a characteristic anisotropic line shape, from which the shielding tensor elements are extracted. However for these relaxor ferroelectric materials, the Pb^{2+} ions are in a variety of local environments due to B-site disorder, therefore there are large distributions of both isotropic and anisotropic ^{207}Pb chemical shifts. The distributions of chemical shifts obscure the characteristic anisotropic line shape and result in a broad and featureless NMR line shape; this has been observed for PMN-PSN.[14]

In solid-state NMR, the magic-angle spinning technique (MAS) is usually used to improve the spectral resolution.[15,16] However, for disordered materials such as PMN-PSN, to separate the distribution of isotropic shifts from anisotropic shifts, inaccessibly high sample spinning speeds (~ 50 kHz) would be required. But in effect the two-dimensional phase-adjusted spinning sidebands (2D-PASS) technique is able to achieve "infinite spinning speed" spectra in the sense of isolating isotropic chemical shift information in one dimension, while preserving valuable anisotropic chemical shift information in the second dimension.[17] The 2D-PASS technique has been successfully applied to study chemical bonding of lead in P_2O_5-PbO glasses.[18] This technique is also able to provide valuable insight on the lead chemical bonding and displacements of PMN-PSN perovskites.

II. EXPERIMENT

The samples $(1-x)$PMN/xPSN ($x=0$, 0.1, 0.2, 0.6, 0.7, and 0.9) have been described in previous studies.[11,12] NMR experiments were carried out on a TECMAG APOLLO console with a 7 T OXFORD magnet. A 0.5 M aqueous $Pb(NO_3)_2$ solution was used to tune the spectrometer (Larmor frequency of 62.589 MHz), and then the carrier frequency was increased by 100 kHz before working on the PMN-PSN samples. The duration of a $\pi/2$ pulse was 3 μs and the spectral width was ± 100 kHz. Depending on the amount of sample, 1000–4000 scans were collected. Lead chemical shifts are reported referenced to tetramethyl lead $[Pb(CH_3)_4]$ at 0 ppm; this was done by using the 0.5 M aqueous $Pb(NO_3)_2$ solution as the working reference sample $[-2941$ ppm on the $Pb(CH_3)_4$ scale].[13]

A Varian-Chemagnetics triple-resonance MAS probe with a spinning control module enables the achievement of spinning speeds up to 12 kHz within ± 2 Hz error. The spinning speeds were $\nu_R = 10$ and 5 kHz for MAS and 2D-PASS experiments, respectively. Teflon spacers were placed on both sides of the rotor to keep the samples in the middle,

TABLE I. Three-step phase cycling for the five π pulses of PASS sequence.

ϕ_1 (°)	ϕ_2 (°)	ϕ_3 (°)	ϕ_4 (°)	ϕ_5 (°)
0	0	0	0	0
120	240	120	120	120
240	120	240	240	240

since the amount of samples was not enough to fill the 5 mm rotor. Boil-off from high-pressure liquid-nitrogen dewars was used for bearing and driving gas as well as for temperature control. Lakeshore temperature controller (model DRC-91CA) and a Varian-Chemagnetics variable temperature (VT) stack, which sat on top of the probe, were used to control sample temperatures; the temperature sensor was located near the lower end of the VT stack. In MAS and 2D-PASS experiments, viscous drag by the driving gas causes sample heating. Temperature calibration was performed making use of the sensitive chemical shifts and narrow linewidth of lead nitrate $Pb(NO_3)_2$.[19] The corrections were $T(°C) = 3(\pm 3) + 0.95(\pm 0.1)T_{\text{read}} °C$ and $T(°C) = 15(\pm 3) + 0.93(\pm 0.1)T_{\text{read}} °C$ for $\nu_R = 5$ and 10 kHz, respectively. This calibration has been implicitly performed and all temperatures reported in this paper are actual corrected values.

Longitudinal relaxation times T_1 were measured on static samples using a saturation-recovery sequence; the saturation was created by a comb consisting of 20 $\pi/2$ pulses separated by 100 ms.[20] A refocusing π pulse was applied before detection to shift the signal by 200 μs so as to acquire the full echo. The intensity at the top of echo, $I(t)$, where t was the recovery time, was fit to the equation $I(t) = I_0[1 - \exp(-t/T_1)]$ using a least-squares algorithm. The relaxation of the broad frequency-domain line shapes is anisotropic and the error of the T_1 values was estimated to be ± 0.5 s.

For MAS experiments at $\nu_R = 10$ kHz, Hahn-echo sequence was used with $\tau = 200$ μs separating the $\pi/2$ and the π pulses.

In a 2D-PASS pulse sequence, five π pulses follow the initial $\pi/2$ pulse.[17] We used a modified version with a shifted echo since the free induction decay (FID) died out extremely fast ($T_2^* < 20$ μs);[18] a duration of two rotor periods (with rotor period $T_R = 200$ μs) was added to the delay before the last π pulse, and a duration of one rotor period was added to the delay after that pulse. Sixteen pitches were used to create 16 t_1 increments; the 16-pitch timing table is available in both Refs. 17 and 18. (However, be reminded that Table I in Ref. 18 contains a typo: the entry in row 5, column 3 should have been 0.11573, not 0.15737.) The spinning speed of 5 kHz was sufficiently low to obtain enough spinning sidebands for reliable extraction of anisotropy parameters, yet it must be sufficiently large so that $16\nu_R$ covers all spinning sidebands. Instead of phase cycling each of the five π pulses independently by increment of 120°,[17] which results in 243 steps, a simplified phase-cycling scheme consisting of only three steps was used (Table I). The phases of the π pulses were cycled in such a correlated manner that $\phi_1 - \phi_2 + \phi_3 - \phi_4 + \phi_5 = 0°$ (or 360°), where ϕ_i ($i=1,2,\ldots,5$) is the
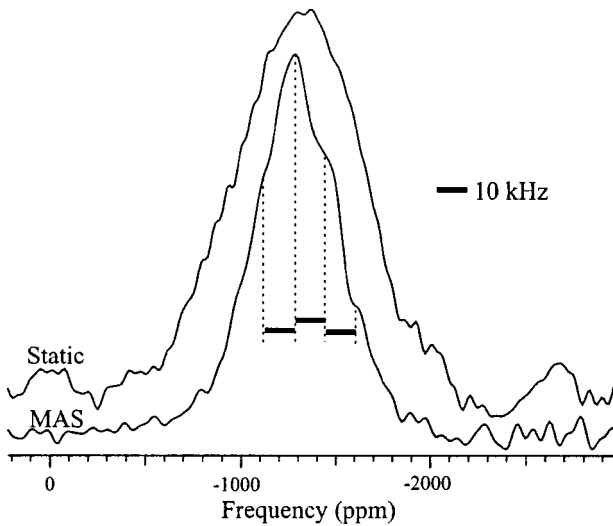
FIG. 1. Static and MAS (10 kHz) ^{207}Pb spectra at 25 °C for ordered 0.3PMN-0.7PSN. Actual sample temperature in MAS experiment was 38 °C due to frictional heating (see Sec. II). Gaussian line broadening of 1 kHz was applied to both before Fourier transform.

phase of the five rf π pulses. The phase of the $\pi/2$ pulse and the receiver reference phase were conventionally cycled in four steps. The same coherence transfer pathway $[(0) \rightarrow (+1) \rightarrow (-1) \rightarrow (+1) \rightarrow (-1) \rightarrow (+1) \rightarrow (-1)]$ is selected by both the original and this simplified phase-cycling schemes. The new phase-cycling scheme was tested on crystalline PbSO$_4$; a clean 2D-PASS spectrum was obtained and the extracted chemical shift parameters were in agreement with literature values.[21] Thus it seems artifacts are well suppressed using this scheme. The recycle delays were at least $3T_1$ for all 2D-PASS experiments.

III. RESULTS

Static and MAS spectra are shown in Fig. 1 for the ordered sample of $x = 0.7$. The static spectrum is very broad [full width at half height (FWHH) 800 ppm, or 50 kHz at 7 T]. Unlike a simple crystalline sample (e.g., PbSO$_4$), whose asymmetric line shape of chemical shielding anisotropy shows characteristic features, this relaxor ferroelectric has a nearly symmetric line shape due to its disordered nature. Magic-angle spinning does significantly narrow the linewidth (reducing it to FWHH of 500 ppm); spinning sidebands with spacing of 10 kHz rotor speed may also be identified as inflections on the line shape. Due to the complexity of the system, there is a distribution of chemical shift anisotropy parameters. MAS speeds of 50 kHz, which exceed the limit of current technology, would be required to completely separate the sidebands from the center band.

The ^{207}Pb longitudinal relaxation times T_1 in $(1-x)$PMN/xPSN are shown in Fig. 2. For PMN within the temperature range investigated (-40 to 60 °C), T_1 decreases with temperature [Fig. 2(a)]; the variation becomes very slow around the temperature for dielectric maximum (-10 °C).[22] For the ordered samples, T_1 has a linear depen-
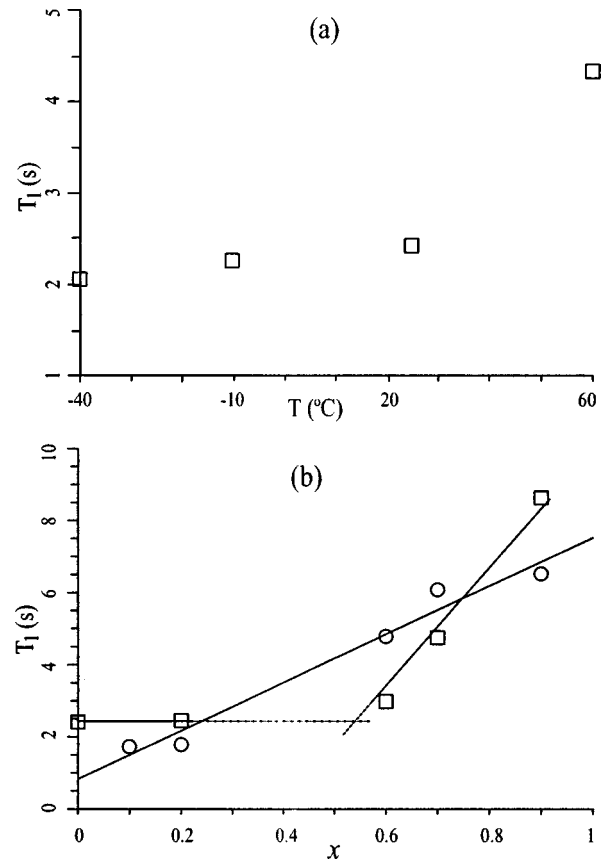

FIG. 2. Lead relaxation time T_1 of $(1-x)$PMN/xPSN. Temperature dependence for PMN (a); concentration dependence at 25 °C (b). Circles are data from ordered samples and squares from disordered materials. The lines in (b) are to guide the eye. Deviation may be ± 0.5 s due to relaxation anisotropy.

dence on concentration x; $T_1(\mathrm{s}) = 0.8(\pm 0.4) + 6.7(\pm 0.7)x$ (with correlation coefficient $R = 0.985$, number of data points $n = 5$) [Fig. 2(b)]. For disordered samples with available concentrations, T_1 is constant, 2.4 s, at low concentrations ($x < 0.5$) and grows rapidly at higher concentrations; $T_1(\mathrm{s}) = -8.4(\pm 0.3) + 18.9(0.9)x$ ($R = 0.999$, $n = 3$) [Fig. 2(b)].

A. 2D-PASS: Isotropic chemical shift

In the 2D-PASS spectrum, the chemical shift isotropy and anisotropy are separated into horizontal and vertical dimensions, respectively. The spectrum of PMN at 27 °C (Fig. 3) reveals a continuous distribution of chemical shift parameters; the projection onto the isotropic dimension offers the distribution of isotropic chemical shifts, which may be fit by a Gaussian line shape with mean $\mu(\delta_{\mathrm{iso}}) = -1343$ ppm and standard deviation $\sigma(\delta_{\mathrm{iso}}) = 206$ ppm (or FWHH $= 484$ ppm, which is much narrower than the MAS linewidth FWHH ≈ 700 ppm). Based on 21 crystalline compounds, Fayon *et al.* have established empirical correlations between isotropic chemical shift and structural parameters,

$$\delta_{\mathrm{iso}} \, (\mathrm{ppm}) = 20854 - 8669.0 r_{\mathrm{Pb-O}} \, (\text{Å}),$$

$$\delta_{\mathrm{iso}} \, (\mathrm{ppm}) = 622.8 - 349.7 \, \mathrm{CN}, \qquad (2)$$
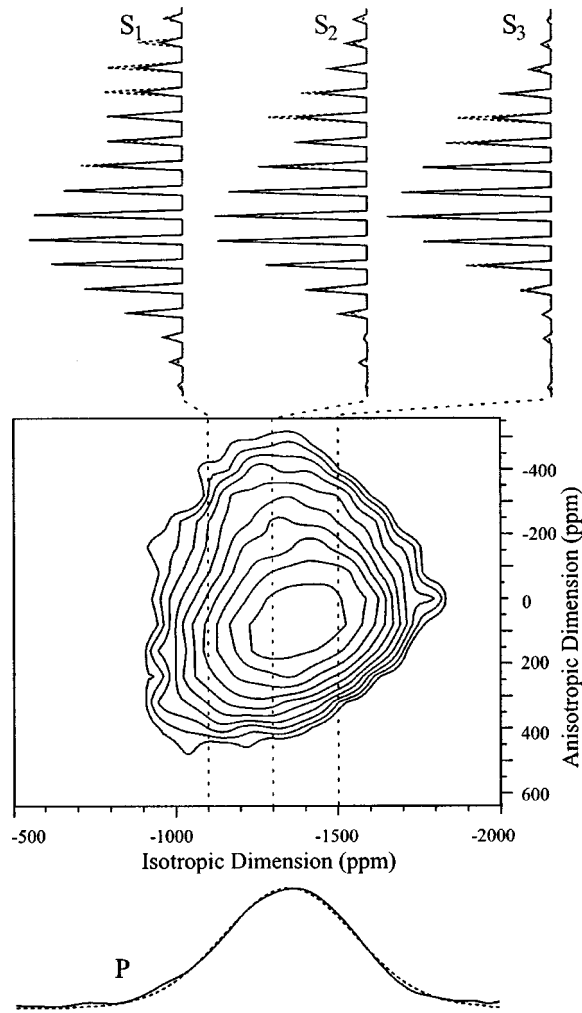
FIG. 3. ^{207}Pb 2D-PASS spectrum of PMN at 27 °C. Gaussian line broadening of 500 Hz was applied in the isotropic dimension. Ten contour levels start with 80% and decrease by factor 0.8. The projection (solid line) onto the isotropic dimension (P) is plotted with a Gaussian fit (dotted line) with center -1343 ppm and FWHH 484 ppm. Three slices along the anisotropic dimension (S_1, S_2, and S_3 at $\delta_{iso} = -1100, -1300,$ and -1500 ppm, respectively) are plotted with fits (in dotted lines) to the spinning sidebands using program DMFIT (Ref. 23); the anisotropic chemical shift parameters are $\delta_{aniso} = -574, -455,$ and -367 ppm and $\eta = 0.6, 0.65,$ and 0.85 for S_1, S_2, and S_3, respectively.

where r_{Pb-O} is the effective Pb-O bond length and CN is the effective coordination number.[24] The linear dependence on CN has been observed only for CN$\geq$7 while δ_{iso} is more scattered for materials with lower coordination number.[24] However, for the PMN-PSN solid solutions, all of which have perovskite structure, the effective coordination number thus calculated should be reasonable. For the isotropic projection of PMN at 27 °C, $\mu(\delta_{iso}) = -1343$ ppm and $\sigma(\delta_{iso}) = 206$ ppm of the Gaussian fit can be translated [Eq. (2)] into distributions of effective bond lengths and coordination numbers; $\mu(r_{Pb-O}) = 2.56$ Å, $\sigma(r_{Pb-O}) = 0.02$ Å and $\mu(CN) = 5.6$, $\sigma(CN) = 0.6$.

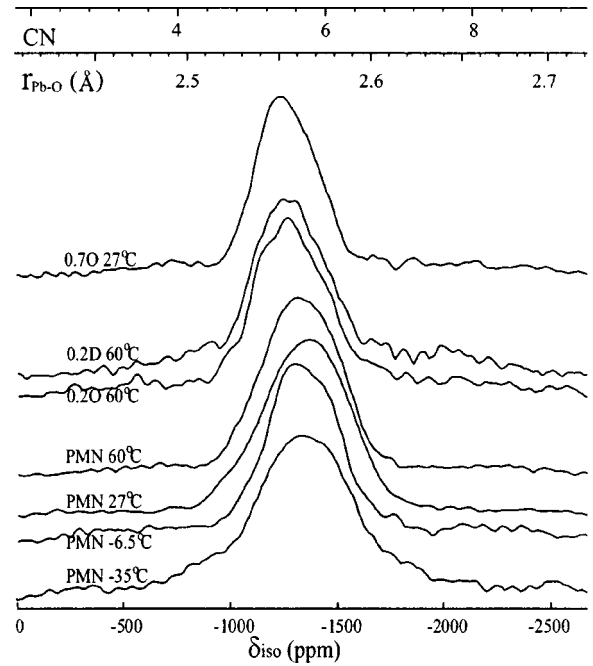The isotropic projections of the 2D-PASS spectra are shown in Fig. 4 for PMN at $-35, -6.5, 27,$ and 60°C, for

FIG. 4. Isotropic projections of ^{207}Pb 2D-PASS spectra for $(1-x)$PMN/xPSN solid solutions. Experiments were performed with spinning speed 5 kHz at $-35, -6.5, 27,$ and 60 °C for PMN, at 60 °C for ordered and disordered samples of $x = 0.2$, and at 27 °C for ordered sample of $x = 0.7$; temperatures have been calibrated as stated in Sec. II. The two axes on top are for conversions to the effective Pb-O distance and coordination number according to Eq. (2).

$x = 0.2$ both ordered and disordered at 60 °C, and for $x = 0.7$ ordered at 27 °C. There are small inflections indicating more structural detail. If these features are ignored, all but one projection may be fit with one Gaussian line shape; only for PMN at -35 °C is a second Gaussian line shape needed to simulate the broad underlying distribution. The fit parameters are listed in Table II. For PMN at temperatures from -6.5 to 60 °C, the mean isotropic chemical shift has a temperature coefficient of $+0.15$ ppm/°C. Similar temperature coefficient of $+0.126$ ppm/°C for PbTiO$_3$ has been reported (over the range -150 to 60 °C); this is attributed to a very small volume expansion that results in the slight changes of Pb-O distance.[25] The standard deviation $\sigma(\delta_{iso})$ has a temperature coefficient of $+0.18$ ppm/°C over the range -6.5 to 60 °C. Lowering the temperature results in larger mean effective Pb-O distance $\mu(r_{Pb-O})$ [and effective coordination number $\mu(CN)$] but smaller distribution width $\sigma(r_{Pb-O})$ [and $\sigma(CN)$]. For PMN at -35 °C, the distribution curve has to be fit with two components, each with about 50% integral intensity. Both components have the same $\mu(\delta_{iso}) = -1347$ ppm, which is very close to -1348 ppm determined at -6.5 °C; this agrees with the fact that the perovskite unit-cell parameters of PMN barely change below room temperature.[26] Component A is narrow and has $\sigma(\delta_{iso}) = 192$ ppm, while component B is broad and has $\sigma(\delta_{iso}) = 425$ ppm. The broad component B at -35 °C does not relate to paraelectric to ferroelectric phase transition of PMN, which happens around 210 K.[27] But PMN has a di-

TABLE II. Gaussian fit parameters for the isotropic projections of 2D-PASS spectra for $(1-x)$PMN/xPSN (see Fig. 4, for example).

Sample and temperature (°C)		δ_{iso} (ppm) [a]		$r_{\text{Pb-O}}$ (Å) [b]		CN [b]	
		μ	σ	μ	σ	μ	σ
0.7O and 27		−1265	169	2.5515	0.0195	5.40	0.48
0.2D and 60		−1279	206	2.5531	0.0238	5.44	0.59
0.2O and 60		−1273	199	2.5524	0.0230	5.42	0.57
0D and 60		−1338	213	2.5599	0.0246	5.61	0.61
0D and 27		−1343	206	2.5605	0.0238	5.62	0.59
0D and −6.5		−1348	201	2.5611	0.0232	5.64	0.58
0D and −35 [c]	A	−1347	192	2.5610	0.0221	5.63	0.55
	B	−1347	425	2.5610	0.0490	5.63	1.22

[a]Error for δ_{iso} is estimated as 5 ppm, which propagates to 6×10^{-4} Å for $r_{\text{Pb-O}}$ and 0.01 for CN, according to Eq. (2).

[b]The mean $\mu(\delta_{\text{iso}})$ and standard deviation $\sigma(\delta_{\text{iso}})$ for isotropic chemical shift distribution are translated into distribution parameters of effective Pb-O bond length $r_{\text{Pb-O}}$ and effective coordination number CN using Eq. (2).

[c]Only PMN at −35 °C needs two components; 49% A + 51% B.

electric maxima around −10 °C,[22] which is attributed to interactions and/or dynamics of nanoclusters.[28,29] It is thus possible that component B arises from chemically ordered nanoclusters.

We emphasize that the variation of the mean isotropic chemical shift $\mu(\delta_{\text{iso}})$ is only −10 ppm over the range +60 to −6.5 °C, and the empirical correlation is not accurate enough to estimate the real variation of bond length corresponding to a 10 ppm shift. The correlation is probably good enough to be used for larger chemical shift variations observed in the concentration dependence.

The concentration dependence may be found by comparing isotropic projections at identical temperatures; PMN and $x=0.2$ at 60 °C, and PMN and $x=0.7$ at 25 °C. Both mean $\mu(r_{\text{Pb-O}})$ and distribution $\sigma(r_{\text{Pb-O}})$ decrease as the PSN concentration x increases. This means that the Pb-O length does not scale in proportion to the perovskite cell parameter, which increases with x (perovskite cell parameters are 4.050 and 4.075 Å for PMN and PSN, respectively).[10,26] This tells us that as the perovskite cell becomes larger, the Pb^{2+} shifts further away from the ideal position, reflecting an increase of the local polar character due to the Mg^{2+}/Sc^{3+} substitution (which results in shortening the shortest Pb-O bond lengths and increasing the longest Pb-O bond lengths).

The parameters for ordered and disordered samples of $x=0.2$ are close. Disorder seems to result in slight increases by around 0.001 Å in both the mean $\mu(r_{\text{Pb-O}})$ and distribution $\sigma(r_{\text{Pb-O}})$ of bond lengths.

B. 2D-PASS: Anisotropic chemical shift

To retrieve chemical shift anisotropy (CSA) from a 2D-PASS spectrum, slices are taken along the anisotropic dimension and catenated with zeros to give spinning sidebands; the intensities of sidebands are then fit with the Herzfeld and Berger algorithm.[30] For example for PMN at 27 °C in Fig. 3, the fitted CSA parameters (δ_{aniso}, η) are (−574 ppm, 0.6), (−455 ppm, 0.65), and (−367 ppm, 0.85) for slices taken

at $\delta_{\text{iso}}=-1100$, −1300, and −1500 ppm, respectively. With increasing δ_{iso}, that is, decreasing bond length $r_{\text{Pb-O}}$ [Eq. (2)], the chemical shift anisotropy $|\delta_{\text{aniso}}|$ increases. This correlation implies that the Pb-O bonds vary from a more ionic environment (longer bond length, lower anisotropy) to a more covalent environment (shorter bond length, higher anisotropy).[18] Thus the chemical shift tensor provides detailed information on electronic bonding.

The principal values of the CSA tensor for PMN are calculated using Eq. (1) and plotted with respect to δ_{iso} in Fig. 5. Very good linear correlations are found between the individual tensor components δ_{ii}, $i=1,2,3$ and the isotropic chemical shift δ_{iso}; regression analyses give $\delta_{11}=940(\pm60)+1.42(\pm0.05)\delta_{\text{iso}}$, $\delta_{22}=300(\pm30)+1.17(\pm0.02)\delta_{\text{iso}}$, and $\delta_{33}=-1230(\pm70)+0.41(\pm0.05)\delta_{\text{iso}}$ with $R=0.99$ for δ_{11} and δ_{22} and $R=0.97$ for δ_{33}.

For PMN at −6.5, 27, and 60 °C, the CSA principal components δ_{11} and δ_{22} increase while δ_{33} decreases as tempera-

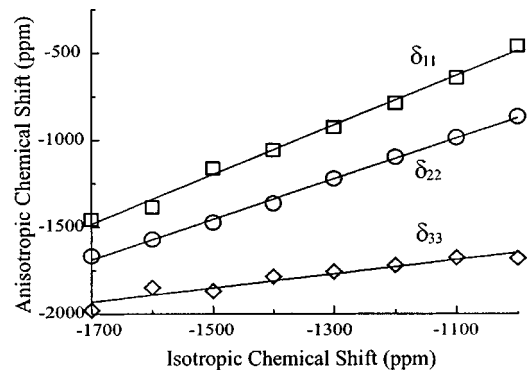FIG. 5. Correlation between anisotropic and isotropic chemical shifts. Data are sampled every 100 ppm from $\delta_{\text{iso}}=-1700$ to −1000 ppm from the 2D-PASS spectrum of PMN at 27 °C (Fig. 3). Errors are about the size of symbol. The regressions are $\delta_{11}=940(\pm60)+1.42(\pm0.05)\delta_{\text{iso}}$, $\delta_{22}=300(\pm30)+1.17(\pm0.02)\delta_{\text{iso}}$, and $\delta_{33}=-1230(\pm70)+0.41(\pm0.05)\delta_{\text{iso}}$.
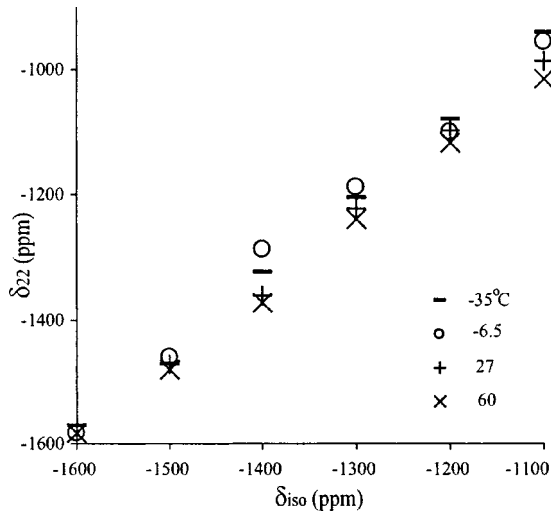
FIG. 6. The temperature dependence of the δ_{22} component of the chemical shielding tensor for PMN at four different temperatures.

FIG. 7. Tetragonal structure of PbTiO$_3$ at room temperature. Lattice parameters $a = 3.904$ Å, $c = 4.105$ Å (Ref. 31). With respect to Ti sublattice, oxygen ions are displaced by $+0.3$ Å in [001] direction and Pb ions are displaced by -0.1 Å (Ref. 10). The 6s lone-pair electrons of Pb^{2+} are schematic depicted.

ture increases; the maximum difference is around 80 ppm. The principal components at -35 °C are between those at -6.5 and 27 °C. In Fig. 6 the temperature dependence of the δ_{22} component is shown.

However, no clear concentration dependence is seen. The principal components at 60 °C for PMN are larger at some δ_{iso} values but smaller at other values than those for $x = 0.2$ (both ordered and disordered). The same pattern is seen when comparing PMN at 27 °C and $x = 0.7$ (ordered).

IV. DISCUSSION

A. Pb-O bonding environments

For PMN-PSN, the measured isotropic and anisotropic chemical shifts suggest that the Pb-O bonds in the system are not strongly covalent. For ionic compounds, weak chemical shift anisotropies and large negative ^{207}Pb isotropic shifts in the range from -2000 to -3500 ppm are observed. In contrast, a more covalent bonding state (for example, oxides and silicates) gives rise to more positive isotropic shifts in the range from -500 to $+1500$ ppm associated with very large chemical shift anisotropies $\delta_{aniso} \sim -2000$ ppm, which reflect the steric effect of the Pb^{2+} lone-pair electrons which preclude a (spherical) symmetric environment with short Pb-O bond lengths.[24] Thus for PMN-PSN, the δ_{iso} range from -1800 to -900 ppm and the δ_{aniso} range -700 to -230 ppm indicate that the Pb-O bonding environments are midway between typical ionic and typical covalent.

The asymmetry parameter η in PMN-PSN ranges from 0.5 to 1; this also supports the above statement concerning Pb-O bonding environments. For example, in lead oxides and silicates (typical covalent compounds), Pb lies at the apex of a PbO$_4$ pyramid (one-sided coordination) and the shielding tensor is close to axially symmetric ($\eta \approx 0$). On the other hand, in lead nitrate (a typical ionic compound), Pb is 12-fold coordinated by oxygen atoms with large Pb-O bond lengths but the shielding tensor is also axially symmetric.
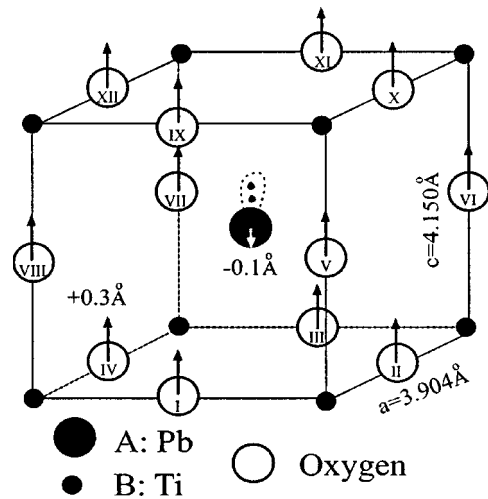
For each sample, the distributions of chemical shift parameters (δ_{iso}, δ_{aniso}, and η) agree with the fact that there is a variety of B^x-O-B^y environments, where B^x and B^y can be any of Mg^{2+}, Sc^{3+}, and Nb^{5+}. In the ABO_3 perovskite structure of Pb(Mg$_{1/3}$Nb$_{2/3}$)O$_3$-Pb(Sc$_{1/2}$Nb$_{1/2}$)O$_3$, the A ion (Pb^{2+}) is in the center of a distorted perovskite cube, the B ions (Mg^{2+}, Sc^{3+}, and Nb^{5+}) are on the eight corners, and the oxygen ions are in the middle of the 12 edges. Thus each Pb^{2+} is surrounded by 12 edges of B^x-O-B^y; the total number of such surroundings is huge. For Mg^{2+}-O-Mg^{2+}, Sc^{3+}-O-Sc^{3+}, Mg^{2+}-O-Sc^{3+}, and Mg^{2+}-O-Nb^{5+}, the average B ion valence is less than four $[(x+y)/2 < 4]$; the Pb-O hybridization is enhanced between the Pb $6s$ and O $2p$ states of such underbonded oxygens.[5,6] While for the remaining cases, the Pb-O hybridization is weaker. Therefore, the distribution of mixed B ions will produce a distribution of Pb-O bond covalence.

B. Measurement of the shortest Pb-O bond length

As the nearest neighbors, the 12 oxygens have the greatest influence on the chemical shifts of lead. To accommodate its lone-pair electrons, Pb^{2+} is usually displaced from the O$_{12}$ center. Being unequally distant from Pb^{2+}, the 12 oxygens have different degrees of influence on the ^{207}Pb chemical shielding tensor. Thus the effective Pb-O bond length deduced from the isotropic chemical shift is a sort of weighted average over the 12 crystallographically inequivalent Pb-O bond lengths. The simple ferroelectric and well-studied PbTiO$_3$ (PT), which is also a perovskite, may help us to build such connections. It is well known that at room temperature PT is tetragonal; lattice parameters $a = 3.904$ Å, $c = 4.105$ Å (Fig. 7).[31] In the [001] direction with respect to the Ti sublattice, oxygen ions are displaced by 0.3 Å and Pb is displaced by -0.1 Å according to neutron time of flight Rietveld refinement.[10] The Pb-O distances split into three

values: 2.5 Å for Pb-O_{I-IV}, 2.8 Å for Pb-O_{V-VIII}, and 3.2 Å for Pb-O_{IX-XII} (see Fig. 7 for oxygen labels). The isotropic chemical shift of PT at room temperature is around -1420 ppm,[25] which corresponds to an effective Pb-O distance of 2.57 Å according to Eq. (2). Thus, the effective Pb-O distance seen by NMR is almost solely determined by the shortest Pb-O distance. For PMN-PSN this shortest Pb-O distance is in the range 2.5–2.6 Å, except for PMN at $-35\,°C$, where the range is 2.45–2.65 Å (Fig. 4). From Fig. 7, it seems CN=4 is appropriate to account for the four closest oxygens on the bottom plane. But the effective coordination number CN=5.8 [according to Eq. (2)] is also very reasonable since the four second-closest oxygens on the middle plane also influence the isotropic chemical shift. Thus, the effective coordination number is slightly bigger than its crystallographic counterpart. The effective CN for PMN-PSN is in the range 4.4–6.8, except for PMN at $-35\,°C$ where the range is 3.6–6.8 (Fig. 4).

C. Lead displacement models

In order to accommodate their lone-pair electrons, Pb^{2+} ions usually shift from high-symmetry positions; a shift of about 0.3–0.4 Å is often seen.[10] An XRD study of PMN shows that the lead displacements may be random in both length and direction; but a single-layer spherical model (radius 0.285 and 0.259 Å for 20 and 300 °C, respectively) adequately describes the XRD data.[9] However in PST, PDF using neutron scattering and x-ray scattering shows that Pb^{2+} ions move (by 0.2 Å) in the [100] direction rather than the macroscopic polarization direction [111].[10] These results are inconsistent. The isotropic projection of 2D-PASS NMR directly measures the distribution of the shortest Pb-O bond length and this allows us to examine the two lead displacement models; their major difference is whether the Pb displacement is in a random direction or a unique direction.

1. Shell model

In the shell model, which is the generalization of the single-layer spherical model, the direction of Pb displacement is random, while the distance from the ideal position has a Gaussian distribution with mean r_0 and standard deviation σ. This was simulated by constructing an ensemble of perovskites with Pb displacements described, and other ions in their ideal positions. The shortest Pb-O bonds were identified and the distribution of the shortest Pb-O distance was plotted. The simulation results are shown in Fig. 8. The mean $r_0 = 0.336$ Å was chosen to roughly align the middle of the simulated curves with the experimental distribution curve for PMN at 27 °C. Simulations were performed with $\sigma = 0.00$, 0.01, 0.02, 0.03, and 0.05. The $\sigma = 0.00$ case corresponds to the single-layer spherical model proposed in the XRD study.[9] However, the simulated distribution curve has several discontinuities and is very asymmetric; it does not resemble the NMR experimental distribution at all. If a small radial distribution is introduced, e.g., $\sigma = 0.01$ and 0.02, the discontinuities become round but the curves are two wide. Increasing radial distribution (e.g., $\sigma = 0.05$) further broadens the simulated distribution curves and this does not help us to match
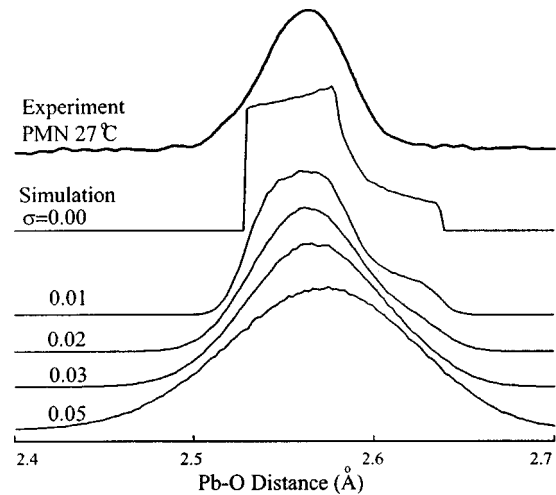

FIG. 8. Shell distribution model for Pb displacement. In the shell model, the direction of Pb displacement is random, while the distance (from the ideal position) has a Gaussian distribution with mean r_0 and standard deviation σ. To roughly align the simulated curves with the experimental distribution curve for PMN at 27 °C, $r_0 = 0.336$ Å is chosen. Simulation has been done for $\sigma = 0.00$, 0.01, 0.02, 0.03, and 0.05 Å. Shell model is unable to reproduce the experimental distribution.

the experimental curve. Thus, shell model is unable to reproduce the experimental distribution.

2. Unique direction model

In the unique direction model, Pb displacement, which is only allowed in a given direction, assumes a Gaussian distribution of mean r_0 and standard deviation σ. The resulting distribution of the shortest Pb-O bond length has a nearly Gaussian line shape. The simulated line shapes fit NMR experiments very well; two examples are shown in Fig. 9 for PMN at 27 °C and $-35\,°C$. All fit parameters are listed in Table III. It turns out that we are unable to discern the direction of the Pb displacement; this model fits experiments equally well with any of the three directions [001], [011], and [111]. However, the distribution parameters strongly depend on the direction; for PMN at 27 °C, $r_0(\sigma) = 0.455$ (0.039), 0.302 (0.023), and 0.381 (0.030) Å for [001], [011], and [111], respectively.

3. Random-bond–random-field model

It is of interest to compare our analysis of 2D-PASS spectra with that of Blinc and co-workers, who interpreted static ^{207}Pb line shapes of single-crystal samples of PMN and PSN in terms of their spherical random-bond–random-field model.[28,29,32] The single-crystal spectra of PMN and PSN include broadening from distributions of dipole-dipole coupling, isotropic chemical shift, and anisotropic chemical shift parameters. They are much broader than our spectra of powdered samples. Presumably this is due to distributions associated with local chemical disorder, which is expected to persist in unannealed single crystals. Blinc and co-workers assume (a) the shift tensors are axially symmetric ($\eta = 0$) and (b) simple linear relations exist between the isotropic
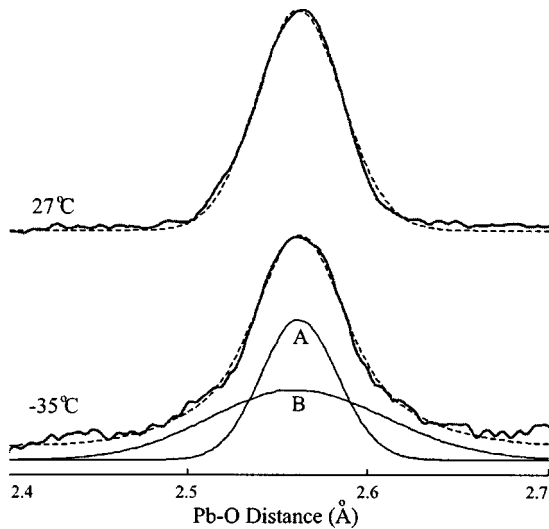
FIG. 9. Unique direction model for the distribution of the Pb displacement. In this model, the displacement of Pb is along a single specified direction and has a Gaussian distribution in distance from ideal position: mean r_0 and standard deviation σ. For PMN at 27 °C (bold line), the NMR experimental distribution of the shortest Pb-O distances is fit with model (dashed line) specified in [001] direction and parameters $r_0 = 0.455$ Å and $\sigma = 0.039$ Å. For PMN at -35 °C, the experimental distribution (bold line) is fit with model (dashed line) in [001] direction and the two components (49% A + 51% B, thin solid lines) have parameters $r_0 = 0.454$ Å and $\sigma = 0.035$ Å for A and $r_0 = 0.454$ Å and $\sigma = 0.080$ Å for B.

shift, shift anisotropy, and the instantaneous value of the ordering field. The higher resolution we obtain in PASS experiments permits determination of all three components of the shielding tensor, and demonstrates that assumption (a) is not adequate, since it varies from 0.6 to 0.85 for PMN at 27 °C. Probably, the relatively low resolution of the static ^{207}Pb spectra allows orientational contributions to their linewidth to be fit using the more primitive spherical shell model.[32]

It is possible that the broader Gaussian component we observe for PMN at -35 °C (Fig. 9) is due to polar nano-

clusters in "chemically ordered" regions, in accord with the random-bond–random-field model. If this is so, variable temperature measurements of PASS spectra at higher magnetic fields, from which individual shielding tensor components could be determined separately for the broad and narrow components, might provide a less ambiguous experimental separation of chemical shift contributions from local bond distortions and mesoscopic polarization.

V. CONCLUSION

The ^{207}Pb static, MAS, and 2D-PASS NMR experiments have been performed on $(1-x)$PMN/xPSN relaxor ferroelectrics as a function of concentration x; temperature dependence is also studied especially on PMN. The inherent chemical and positional disorder in these materials results in very low resolution in the static and MAS spectra. Only in 2D-PASS spectra can isotropic and anisotropic chemical shifts be separated. The isotropic chemical shift δ_{iso} ranges from -1800 to -900 ppm; the anisotropic chemical shift δ_{aniso} ranges from -700 to -230 ppm; the asymmetry parameter η ranges from 0.5 to 1, thus the shielding tensor is far from axially symmetric. The isotropic chemical shift is empirically related to the effective NMR Pb-O distance, which decreases upon increasing the perovskite cell parameter by increasing either the concentration x or temperature. This is because the Pb ion moves further away off center as the cell parameter increases. Strong linear correlations between isotropic and anisotropic chemical shifts show that Pb-O bonds vary from more ionic to more covalent environments. The existence of various Pb-O bonds is a result of the distribution of mixed B ions.

By comparing the crystallographic and NMR study for PbTiO$_3$, the NMR effective Pb-O distance is found to correlate with the shortest Pb-O bond length (among the 12 Pb-O bonds in a perovskite cell). Thus the distribution of isotropic chemical shifts is essentially the distribution of the shortest Pb-O bond length. This distribution is used to examine two competing models of Pb displacement; the direction of dis-

TABLE III. Parameters of unique direction model for Pb displacement. For $(1-x)$PMN/xPSN ordered and disordered samples, the NMR experimental shortest Pb-O distributions are fit with this model at three special directions (see Fig. 9 for example).

Sample and temperature (°C)		[001]		[011]		[111]	
		r_0 [a]	σ [b]	r_0	σ	r_0	σ
0.7O and 27		0.473	0.032	0.313	0.020	0.394	0.025
0.2D and 60		0.468	0.038	0.310	0.022	0.391	0.030
0.2O and 60		0.468	0.038	0.310	0.022	0.391	0.030
0D and 60		0.456	0.041	0.303	0.025	0.382	0.033
0D and 27		0.455	0.039	0.302	0.023	0.381	0.030
0D and -6.5		0.454	0.037	0.302	0.022	0.380	0.029
0D and -35 [c]	A	0.454	0.035	0.301	0.021	0.380	0.028
	B	0.454	0.080	0.301	0.055	0.380	0.067

[a]The mean of the Gaussian distribution of the displacement, precision 0.001 Å.
[b]The standard deviation of the Gaussian distribution of the displacement, precision 0.001 Å.
[c]Only PMN at -35 °C needs two components; 49% A + 51% B.

placement is random in the spherical model but specific in the unique direction model. The spherical model yields an asymmetric distribution curve which is unable to fit the observed distribution of the shortest Pb-O bond length. The unique direction model yields a Gaussian distribution curve which can fit the observed distribution. However, it is unable to discern the direction of the Pb displacement; this model fits experiments equally well with any given direction. The distribution parameters strongly depend on the direction; for PMN at 27 °C, $r_0(\sigma) = 0.455$ (0.039), 0.302 (0.023), and 0.381 (0.030) Å for [001], [011], and [111], respectively, where r_0 and σ are, respectively, the mean and standard deviation of the Gaussian distribution of the Pb displacement from the ideal position. For PMN at -35 °C (below the dielectric maxima temperature -10 °C), the distribution curve has to be fit with two components with the same r_0 but different σ; the [011] direction model gives $r_0 = 0.301$ Å and $\sigma = 0.021$ and 0.055 Å for the narrow and broad components, respectively.

Ab initio calculations of local structure indicate that the excellent piezoelectric response of lead zirconate/lead titanate solid solutions (PZT) is due mostly to displacement of the lead cations, and the direction of these displacements is sensitive to cation ordering and overall macroscopic polarization of the material.[33] In that study, structural motifs were separated into environment-independent crystal chemistry requirements (such as the preferred cage size for BO_6 octahedral cages), and nontransferable ways of achieving these requirements in particular solid solutions. Analogous calculations have not yet been done for PMSN, although the

^{93}Nb NMR results in the preceding works could greatly facilitate the construction of realistic model supercells.[11,12]

Despite the absence of detailed *ab initio* calculations, consideration of the actual distribution of nearest *B*-site neighbor configurations, determined quantitatively for the first time in our previous ^{93}Nb NMR study,[11] and *A*-site uniaxial displacements revealed by ^{207}Pb NMR, together provide general confirmation of the ideas proposed by Cooper *et al.* regarding the microscopic origins of piezoelectric and relaxor ferroelectric behavior.[33] Thus, in mixed configurations in PMSN, lead will distort away from the larger Mg and Sc cations and toward the Nb cations. Just as in PZT, the Pb cation may not distort in the [111] direction directly toward the small but toward highly charged Nb cation, and the direction of distortion will be a sensitive function of the identity of all the surrounding *B*-site cations. Thus, it is likely that the disordered configurations labeled D_1 and D_2 in the ^{93}Nb NMR studies,[11,12] which involve at Nb cations with at least one nearest *B*-site Nb neighbor, also involve large off-center *A*-site distortions in many different directions. This may explain why D_1 and D_2 must account for a significant fraction of the material ($>20\%$) if relaxor behavior is to occur.[11]

*Corresponding author. Email address: gina@physics.wm.edu

[1] L.E. Cross, Ferroelectrics **151**, 305 (1994).

[2] R.E. Newnham, NIST Spec. Publ. **804**, 39 (1996).

[3] K. Uchino, *Piezoelectric Actuators and Ultrasonic Motors* (Kluwer Academic, Boston, 1996).

[4] S.-E. Park and T.R. Shrout, J. Appl. Phys. **82**, 1804 (1997).

[5] B.P. Burton and E. Cockayne, Phys. Rev. B **60**, R12 542 (1999).

[6] B.P. Burton, J. Phys. Chem. Solids **61**, 327 (2000).

[7] Z. Wu and H. Krakauer, Phys. Rev. B **63**, 184113 (2001).

[8] G.A. Samara, Solid State Phys. **56**, 239 (2001).

[9] S. Vakhrushev, S. Zhukov, G. Fetisov, and V. Chernyshov, J. Phys.: Condens. Matter **6**, 4021 (1994).

[10] W. Dmowski, M.K. Akbas, P.K. Davies, and T. Egami, J. Phys. Chem. Solids **61**, 229 (2000).

[11] G.L. Hoatson, D.H. Zhou, F. Fayon, D. Massiot, and R.L. Vold, Phys. Rev. B **66**, 224103 (2002).

[12] D.H. Zhou, G.L. Hoatson, and R.L. Vold, J. Magn. Reson. **167**, 242 (2004).

[13] Y.-S. Kye, S. Connolly, B. Herreros, and G.S. Harbison, Main Group Metal Chem. **22**, 373 (1999).

[14] M.D. Glinchuk, V.V. Laguta, I.P. Bykow, S. Nokhrin, V.P. Bovtun, M.A. Leschenko, J. Rosa, and L. Jastrabik, J. Appl. Phys. **81**, 3561 (1997).

[15] U. Haeberlen and J.S. Waugh, Phys. Rev. **175**, 453467 (1968).

[16] M.M. Maricq and J.S. Waugh, J. Chem. Phys. **70**, 3300 (1979).

[17] O.N. Antzutkin, S.C. Shekar, and M.H. Levitt, J. Magn. Reson., Ser. A **115**, 7 (1995).

[18] F. Fayon, C. Bessada, A. Douy, and D. Massiot, J. Magn. Reson. **137**, 116 (1999).

[19] A. Bielecki and D.P. Burum, J. Magn. Reson., Ser. A **116**, 215 (1995).

[20] E. Fukushima and S.B. Roeder, *Experimental Pulse NMR: A Nuts and Bolts Approach* (Addison-Wesley, London, 1981).

[21] P. Zhao, S. Prasad, J. Huang, O.J.J. Fitzgerald, and J.S. Shore, J. Phys. Chem. B **103**, 10617 (1999).

[22] J. Chen, H.M. Chan, and M.P. Harmer, J. Am. Ceram. Soc. **72**, 593 (1989).

[23] D. Massiot, F. Fayon, M. Capron, I. King, S. Le Calve, B. Alonso, J.-O. Durand, B. Bujoli, Z. Gan, and G. Hoatson, Magn. Reson. Chem. **40**, 70 (2002).

[24] F. Fayon, I. Farnan, C. Bessada, J. Coutures, D. Massiot, and J.P. Coutures, J. Am. Chem. Soc. **119**, 6837 (1997).

[25] D. Bussian and G. Harbison, Solid State Commun. **115**, 95 (2000).

[26] P. Bonneau, P. Garnier, G. Calvarin, E. Husson, J.R. Gavarri, A.W. Hewat, and A. Morell, J. Solid State Chem. **91**, 350 (1991).

[27] R. Sommer, N.K. Yushin, and J.J. van der Klink, Phys. Rev. B **48**, 13 230 (1993).

[28] R. Blinc, A. Gregorovic, B. Zalar, R. Pirc, V.V. Laguta, and M.D. Glinchuck, J. Appl. Phys. **89**, 1349 (2001).

[29] V.V. Laguta, M.D. Glinchuk, S.N. Nokhrin, I.P. Bykov, R. Blinc, A. Gregorovic, and Z.B. Zalar, Phys. Rev. B **67**, 104106 (2003).

[30] J. Herzfeld and A.E. Berger, J. Chem. Phys. **73**, 6021 (1980).

[31] G. Jona, Francoand Shirane, *Ferroelectric Crystals*, The International Series of Monographs on Solid State Physics Vol. 1 (Pergamon Press, New York, 1962).

[32] R. Blinc, A. Gregorovic, B. Zalar, R. Pirc, V.V. Laguta, and M.D. Glinchuck, Phys. Rev. B **63**, 024104 (2001).

[33] V.R. Cooper, I. Grinberg, N.R. Martin, and A.M. Rappe, in *Fundamental Physics of Ferroelectrics 2002*, edited by R.E. Cohen, AIP Conf. Proc. No. 626 (AIP, Washington, DC, 2002), pp. 26–35.